AGU PUBLICATIONS

JGR

Journal of Geophysical Research: Space Physics

RESEARCH ARTICLE
10.1002/2017JA024365

Key Points:
- Daytime MSTIDs at conjugate regions
- Mechanisms responsible for daytime electrified MSTIDs
- Gravity wave induced electric field role in daytime MSTIDs

Correspondence to:
O. F. Jonah,
olujonah@mit.edu

Citation:
Jonah, O. F., E. A. Kherani, and E. R. De Paula (2017), Investigations of conjugate MSTIDS over the Brazilian sector during daytime, *J. Geophys. Res. Space Physics*, *122*, 9576–9587, doi:10.1002/2017JA024365.

Received 15 MAY 2017
Accepted 20 JUL 2017
Accepted article online 28 JUL 2017
Published online 8 SEP 2017

©2017. American Geophysical Union. All Rights Reserved.

Investigations of conjugate MSTIDS over the Brazilian sector during daytime

O. F. Jonah[1,2], E. A. Kherani[1], and E. R. De Paula[1]

[1]National Institute for Space Research (INPE), São José Dos Campos, Brazil, [2]Haystack Observatory, Massachusetts Institute of Technology, Westford, Massachusetts, USA

Abstract This study focuses on the daytime medium-scale traveling ionospheric disturbances (MSTIDs) observed at conjugate hemispheres. It is the first time that the geomagnetical conjugate daytime MSTIDs are observed over the South America sector. To observe the MSTID characteristics, we used detrended total electron content (TEC) derived from Global Navigation Satellite Systems receivers located at Brazilian sector covering the Northern and Southern Hemispheres along the same magnetic meridian. The geographic grid of 1°N to 14°S in latitude and 60°S to 50°S in longitude was selected for this study. The cross-correlation method between two latitudes and longitudes in time was used to observe the propagation of the MSTID waves. The following features are noted: (a) MSTIDs are well developed at both hemispheres; (b) the peak MSTIDs amplitudes vary from one hemisphere to another; hence, we suppose that MSTIDs generated in Southern Hemisphere or Northern Hemisphere mirrored in the conjugate hemisphere; (c) the gravity wave-induced electric fields from one hemisphere map along the field lines and generate the mirrored MSTIDs in the conjugate region. To investigate the hemispheric mapping mechanism, a rough approximation for the integrated field line conductivity ratio of *E* and *F* regions is calculated using digisonde *E* and *F* region parameters. We noted that during the period of mapping the decrease in *E* region conductivity results in an increase in total conductivity. This shows that the *E* region was partially short circuited; hence, electric field generated at *F* region could map to the conjugate hemisphere during daytime: daytime MSTIDs at conjugate regions; mechanisms responsible for daytime electrified MSTIDs; gravity wave-induced electric field role in daytime MSTIDs.

1. Introduction

MSTIDs (medium-scale traveling ionospheric disturbances) are wavelike disturbances in the density and electric field that travel in the ionosphere. They can also be described as the manifestations of atmospheric gravity wave (AGW) in the ionosphere. They play important roles in the dynamics of the Earth's atmosphere such as the coupling between the lower, middle, and upper atmosphere, and they are detrimental to radio wave propagations.

One of the interesting characteristics of these MSTIDs is its possibility of being generated at the conjugate region by the mapping of electric field along the magnetic field lines from the source region. From now on, we refer to this phenomenon as "electrified MSTIDs". *Burnside et al.* [1983] have shown that large electric field could originate at one hemisphere and map along the magnetic field lines to the opposite hemisphere using the incoherent scatter radar measurements. Since then many literature have shown that electric field mapping to the opposite hemisphere can generate conjugate mirrored MSTIDs at opposite hemisphere during nighttime period by using both observations and simulation studies [*Otsuka et al.*, 2004; *Martinis et al.*, 2010; *Duly et al.*, 2014; *Huba et al.*, 2015].

The recent observations by *Otsuka et al.* [2004] have shown geomagnetic conjugate observation, and they explained that the mirrored MSTIDs at both hemispheres are owning to the movement of ionospheric plasma in the direction perpendicular to the magnetic field in both hemispheres, which implies that electric field could be involved in the generation of MSTID at the conjugated region. In their study, they reported a simultaneous observation of MSTIDs at geomagnetic conjugate points using a 630 nm all-sky CCD imager at Sata (31.0°N, 130.7°E; magnetic latitude 24°N) and at Darwin (12.4°S, 131.0°E; magnetic latitude 22°S). It was shown that MSTIDs at Darwin propagated northwestward at almost the same velocity as the MSTIDs observed at Sata with southwestward propagation. The study clearly revealed that the polarization electric field mapped along magnetic field line ($\overrightarrow{B}$) and caused MSTIDs generation at the conjugate hemisphere during nighttime.

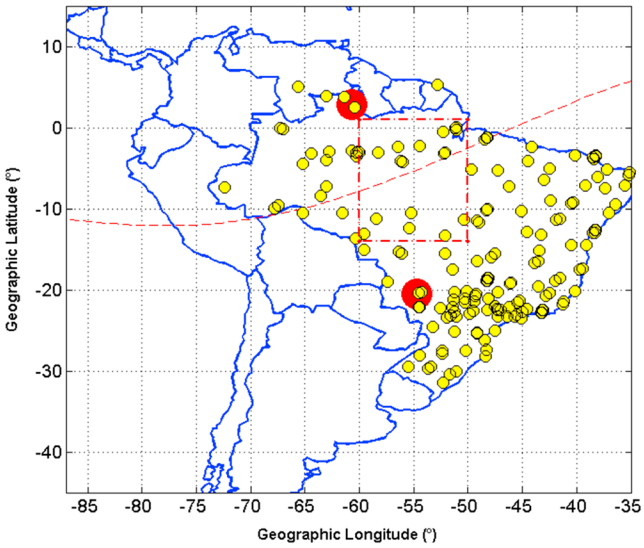

Figure 1. The yellow circles in the red dash-dotted box show the distribution of the GPS receivers used, the red circle shows the stations of the ionogram location, and the red dashed line shows the magnetic equator for December 2014.

Other interesting works are the simulation studies by *Duly et al*. [2014] and *Huba et al*. [2015] using the SAMI3/ESF model. *Huba et al*. [2015] presented a 3-D simulation study of conjugate ionospheric effects associated with the Tohoku-Oki tsunami of 11 March 2001 during nighttime period with input of tsunami-driven gravity wave. It was shown that even though the tsunami-driven gravity wave disturbance was in the Northern Hemisphere, its effects could be observed at the conjugate Southern Hemisphere because the gravity waves induced electric fields mapped along the magnetic field lines to the conjugate region and caused the observed ionospheric disturbances (MSTID signature) in the TEC and airglow emission in the Northern Hemisphere. While *Duly et al*. [2014] presented synthetic observations of MSTIDs in total electron content (TEC), integrated 630.0 nm airglow emission, $E \times B$ drift, electron density, and their results show the signature of MSTIDs at magnetic conjugate hemispheres. The recent study by *Valladares and Sheehan* [2016] also investigated the spatial variability and dynamics of nighttime MSTIDs and mapping characteristics of electrified MSTIDs from one hemisphere to the conjugate hemisphere on two days in August 2012. In line with the above discussions, the viable explanation from instrument like airglow images by *Fukushima et al*. [2012] and the observation work from satellite measurements by *Jonah et al*. [2016, and references therein] equally showed that generation of MSTIDs are attributed to gravity wave-induced electric field. The study of *Kelley and Fukao* [1991] also suggests that gravity waves could produce required density structures which are explained by the Perkins instability [*Perkins*, 1973], and *Duly et al*. [2014] investigated the possibility that the Perkins instability was responsible for MSTIDs. Ultimately, another important characteristic of MSTIDs, as observed in ΔTEC amplitude, is the preferential propagation toward equator which have been explained by authors like *Kotake et al*. [2007] and *Jonah et al*. [2016] as due to the neutral particles oscillation parallel to $\overrightarrow{B}$ being larger for gravity wave traveling equatorward than those traveling in other directions. For in-depth discussion about gravity waves, readers are referred to the recent studies by *Fritts and Alexander* [2003], *Vadas and Liu* [2009], and *Yigit and Medvedev* [2015].

In the present study, we use observational TEC disturbance from Global Navigation Satellite Systems (GNSS) data and *hF* from digisonde data to describe the time-varying characteristics of daytime MSTIDs, their mapping structures, and the mechanisms responsible for daytime MSTIDs observed on four days in December 2014; hence, our results represent case studies and do not necessarily represent the general features of MSTIDs, which can only be inferred by studying more such cases. A brief description of the method used in the study is given in section 2. Section 3 presents the results of MSTIDs on four geomagnetic quiet days. Section 4 presents discussions on the mechanism responsible for daytime mapping of electrified MSTIDs which have similar electrodynamics nature/process with the nighttime counterpart. Lastly conclusions are given in section 5.

2. Data Analysis

To carry out our studies of the MSTIDs characteristics, we used detrended TEC (according to equations (1)) at the Brazilian sector along the Northern and Southern Hemispheres geographically (i.e., 0° to 20°S and 60° to

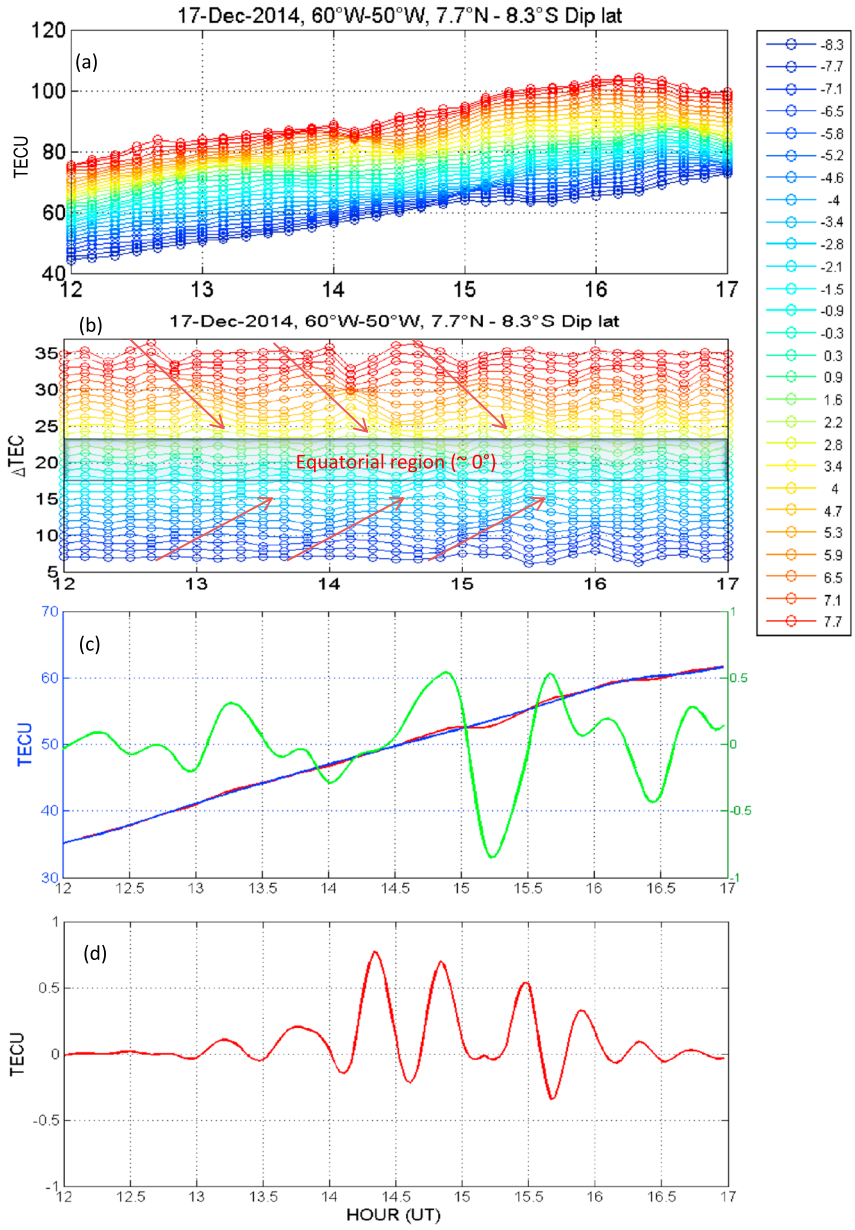

Figure 2. (a) The TEC, (b) the ΔTEC (the red arrows are used to indicate the pattern of the mirrored waves), (c) an example of how detrended TEC was derived, i.e., TEC mean (red color), if the polynomial fit (blue color), and the resultant detrended TEC, (d) while the red curve shows an example of the cross-correlation between two latitudes which represents the MSTID propagation.

45°W) as shown in Figure 1. The latitude coordinates are later converted to geomagnetic coordinates using the International Geomagnetic Reference Field model (2012, https://www.ngdc.noaa.gov/IAGA/vmod/igrf12.f). The GNSS data used for this study were provided by the following databases:

1. SOPAC: Scripts and Permanent Array Centre Garner GPS archive (known as SOPAC GARNER) contains files of observation and navigation from the GPS global network. The database belongs to the International GNSS Service (IGS). It is available at (ftp://garner.ucsd.edu/pub/rinex/).
2. RBMC/IBGE: Brazilian Network for Continuous Monitoring of the Institute of Brazilian Geography and Statistics. The data of this database can be accessed at (ftp://geoftp.ibge.gov.br/RBMC/dados/).

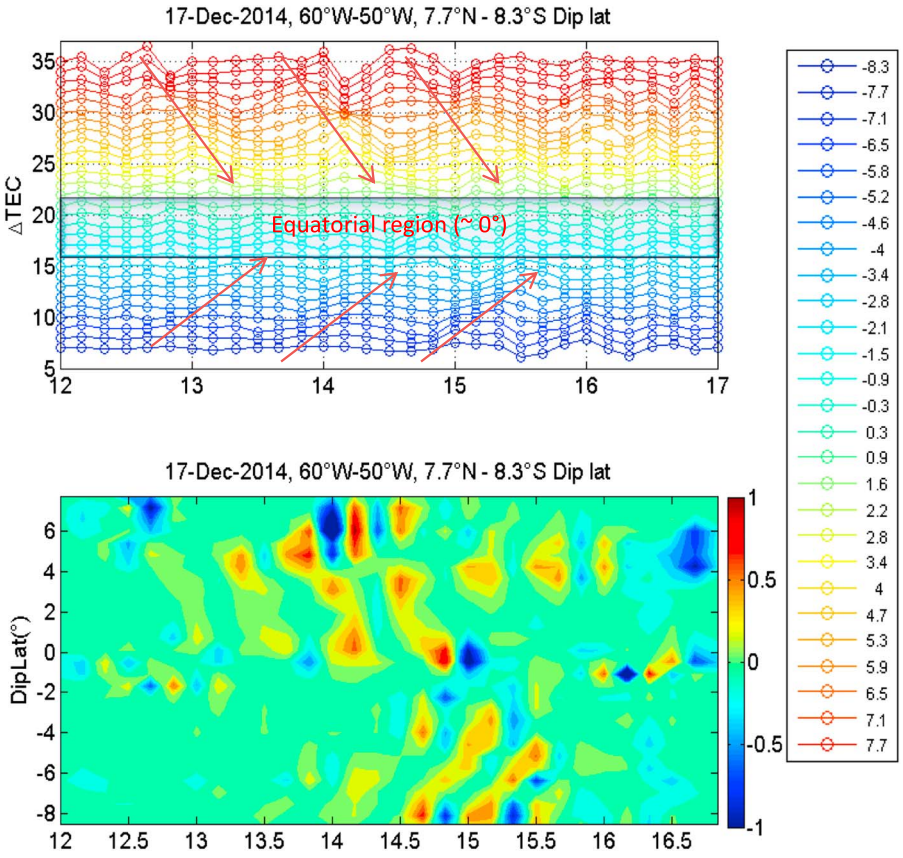

Figure 3. (top) The TEC disturbance in latitude. Each line represents latitude/longitude as indicated in the legend. (bottom) MSTID propagation derived from the cross-correlation coefficients in latitude.

The TEC disturbance (ΔTEC) is derived by subtracting the TEC best fit (TEC_{fit}) from the mean TEC, i.e.,

$$\Delta TEC = \overline{TEC_i} - TEC_{fit}(x,t) \tag{1}$$

where $\overline{TEC_i} = \frac{\sum_{t=1}^{N} TEC_t}{N}$, i represents each latitude or longitude for all times, x is the space (in longitude or latitude), and N is the total number of t. The cross-correlation maps are generated and defined as follows:

$$MSTID_{PROP} = \frac{\Delta TEC(x,t) \times \Delta TEC(x+\Delta x, t+\Delta t)}{(\Delta TEC)^2} \tag{2}$$

where: $\Delta t = 10$ min, $(\Delta x, \Delta t)$ the change in space with time, and $MSTID_{PROP}$ is the cross-correlation coefficient as a function of change in space and time. These cross-correlation maps enable us to identify the waves, if present, by tracking the space and temporal shift of the maximum cross-correlation region. Equation (2) represents the MSTIDs propagation between two latitudes or two longitudes. Detailed explanations are given in *Jonah et al*. [2016].

Note that the MSTIDs are defined as the TEC perturbations (ΔTEC), and an event is defined as a single wave with crest and trough [*Jonah et al*., 2016]. Figure 2 provides the detail information about the measurement of the observed daytime MSTIDs. Figure 2a represents the TEC, Figure 2b represents the detrended TEC which was derived as shown in (Figure 2c, where the blue and red curves represent the polynomial fit and the mean

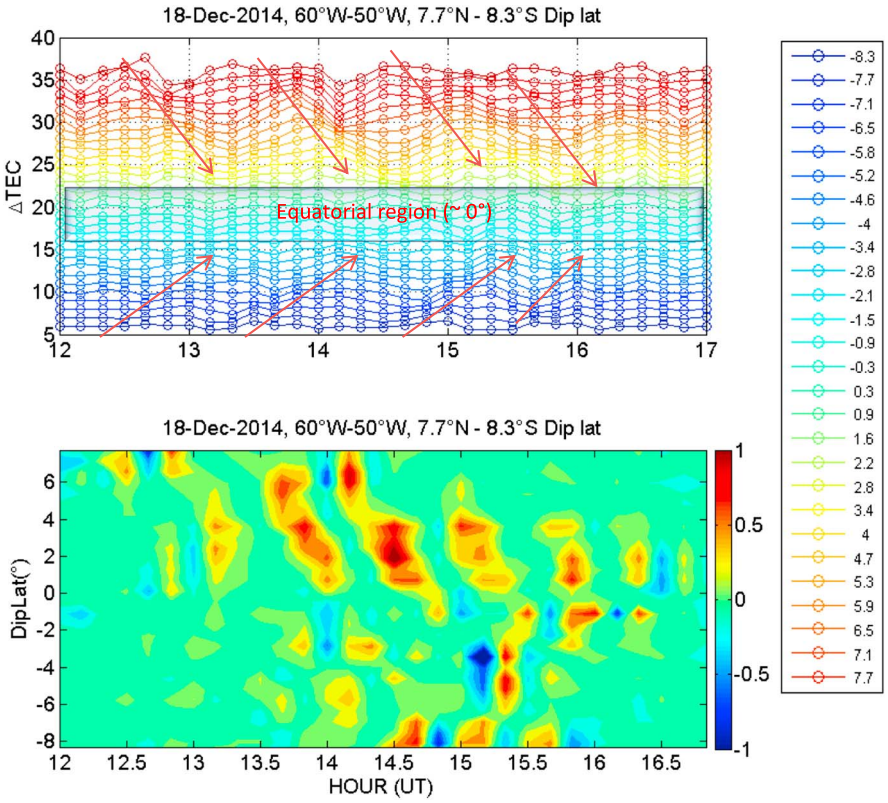

Figure 4. The same as Figure 3 but for day 18.

TEC, respectively, while the green curve is the detrended TEC obtained by equation (1). And lastly, the red curve in Figure 2d shows the MSTIDs propagation between two latitudes as derived from equation (2).

3. Results on Observations

Figures 3a and 3b present the derived TEC disturbances from the GNSS measurements during quiet geomagnetic conditions ($Kp \leq 3$) on 17 December 2014 during 12–17 UT. Figure 3a represents the TEC polynomial fit as a function of ΔTEC (TECU, 1 TECU = 10^{16} electron/m^2) and as function of universal time as derived by equation (1), and it depicts the temporal variations of the TEC disturbance extracted in latitude. Each line plot represents the latitudinal oscillation for each 0.5° latitude. It is important to note that a constant value is added to each ΔTEC (VTEC) value in order to give a clear gap between each latitude line plots. On the other hand, the corresponding cross-correlation maps in latitude as function of universal time are represented by Figure 3b, and it is derived using equation (2). Figures 4–6 represent the same corresponding parameters but for days 18, 27, and 28 December 2014. For easy comprehensive discussion, we refer 17, 18, 27, and 28 December 2014 as D17, D18, D27, and D28, respectively. Note that Brazilian standard time (BST) = UT − 3 h.

We note the following features in Figures 3a–3b on D17: (a) MSTID events oscillate in time with period of 20 to 35 min at both southern and northern regions; (b) the phase of the oscillation shifts in time while going toward the equatorward direction. (c) In most cases corresponding MSTID events maximize sometime during 13–16 UT (10–13 LT), (d) the maxima are observed to commonly shift equatorward with time at both hemispheres, (e) these MSTIDs are well defined and last longer in the Northern than in the Southern Hemisphere. (f) The electrified MSTIDs generated at the Southern Hemisphere or Northern Hemisphere are mirrored in the conjugate hemisphere. (g) The mirrored MSTID structures (at both hemispheres) are centered around the magnetic equator as expected. Qualitatively, similar features are noted during D18, D26, and D27 in Figures 4–6, respectively. Noteworthy quantitative differences are the following: (h) there are more and well-defined electrified MSTIDs events on D27 and D28 with maxima peaks at ~13:30 UT compared to D17 and D18, which show relatively weak/fewer electrified MSTIDs events.

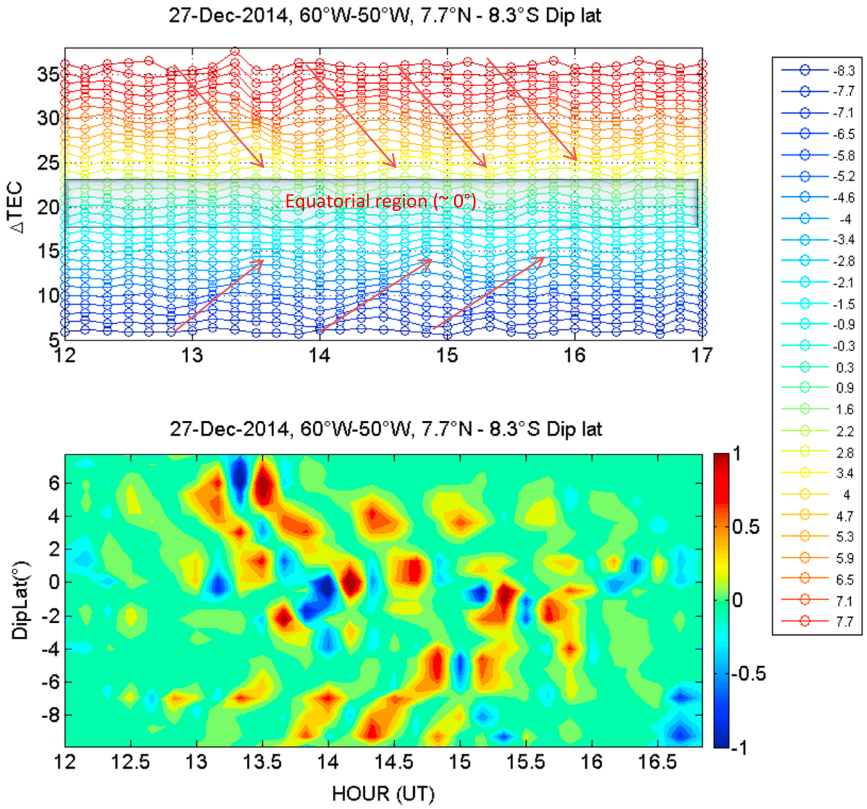

Figure 5. The same as Figure 3 but for day 27.

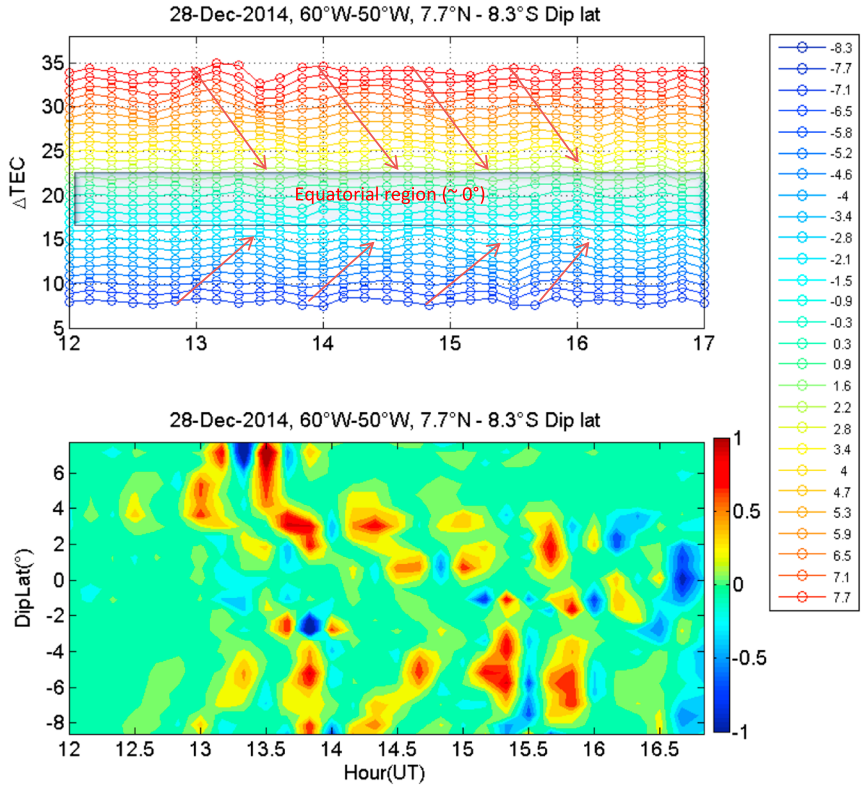

Figure 6. The same as Figure 3 but for day 28.

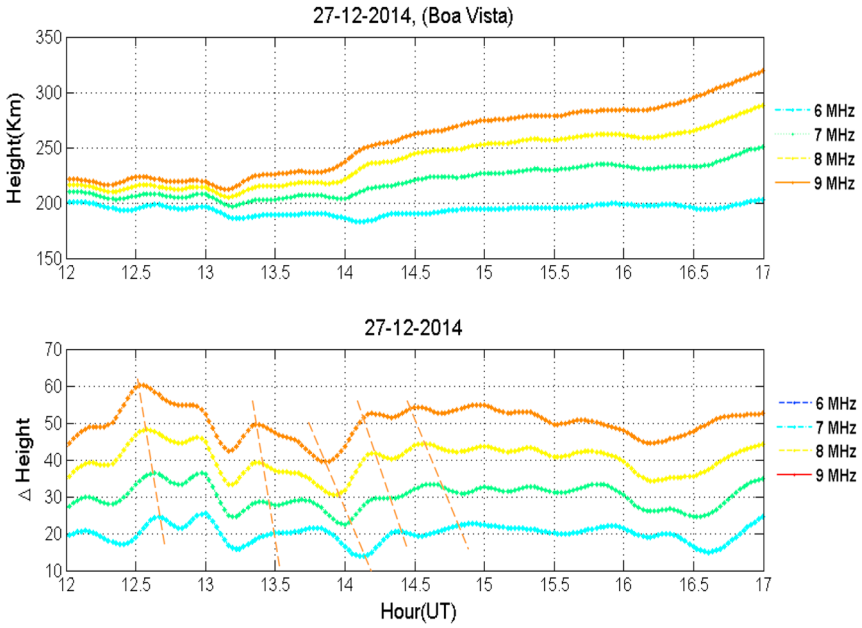

Figure 7. (top) The hF (height) at 6 to 9 MHz for Boa Vista (2.62°N, 60.7°W, dip angle: 22.05°N) as a function of time, (bottom) the Δheight using the similar method of equation (1). The red lines are used to indicate the pattern of the waves.

4. Discussion

4.1. Mechanism Responsible for the Daytime Electrified MSTIDs:

It may be noted that the major features at (a) to (e) (in section 3) are similar to those discussed by *Jonah et al.* [2016] that focused only on the southern MSTIDs. The new important features for this study are mentioned in items (f) to (h), and they are discussed below:

The nighttime MSTIDs observed at the conjugate hemisphere and the mechanisms responsible have been explained by *Otsuka et al.* [2004]. However, it is generally believed that these explanations for nighttime MSTIDs at the conjugate hemisphere are not directly applicable to the daytime MSTIDs at the conjugate hemisphere because their electrodynamics processes are different. Although the conjugate nighttime MSTIDs have been explained by the polarization electric field observed at either hemisphere that mapped along magnetic field to the conjugate hemisphere, there are no explanation in the literatures for mechanism responsible for a simultaneous observation of MSTIDs at conjugate hemisphere during daytime. The polarization electric field exists during nighttime, because electric field generally generated by the *F* region dynamo mechanism is no longer short circuited by the *E* region due to the well-known sunset terminator mechanism [e.g., *Abdu*, 2005]. Moreso, as explained by *Otsuka et al.* [2004], electric current $\vec{J}$ would flow to almost the same direction as $\vec{U} \times \vec{B}$, where $\vec{U}$ is the gravity wave-induced neutral wind. Since $\vec{J}$ traverses the perturbations of integrated Pederson conductivity caused by the wavefront of MSTIDs over one hemisphere, polarization electric fields ($\vec{E}_p$) should be generated to maintain a divergence-free ionospheric current. Thus, $\vec{E}_p$ should be perpendicular to the wavefronts of MSTIDs. *Jonah et al.* [2016, and references therein] have also shown that generation of MSTIDs are attributed to gravity waves-induced electric field. In the consequent discussions, we show that this gravity wave-induced electric fields would map along the field lines and generate the mirrored/electrified MSTIDs in the conjugate region.

4.1.1. Analogous AGW Activity at Conjugate Points

To further investigate the conjugate hemispheric electric field mapping on the observation of daytime electrified MSTIDs at conjugate region, we used the *hF* from the digisondes located at magnetically conjugate points of Boa Vista (2.82°N, 60.7°W, dip angle: 22.05°N) and Campo Grande (20.55°S, 54.7°W, dip angle:

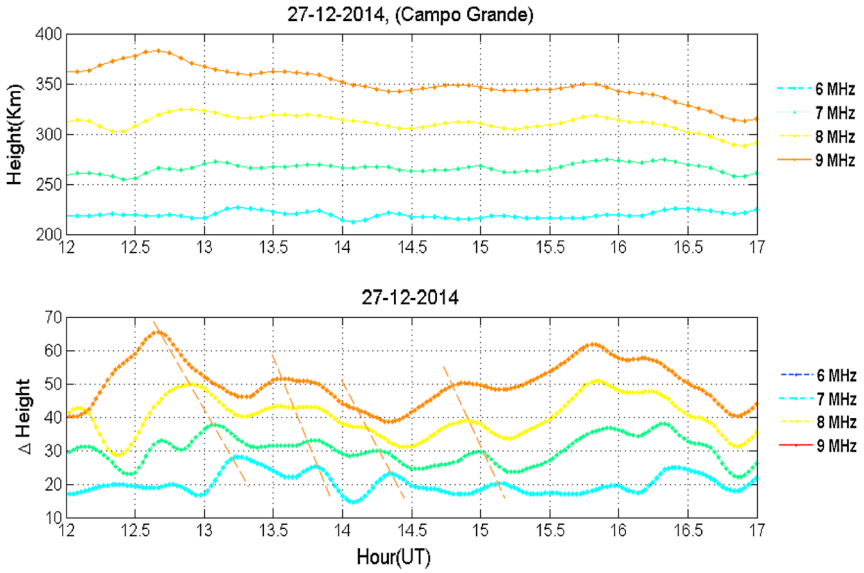

Figure 8. The same as Figure 7 but for Campo Grande (20.55°S, 54.7°W, dip angle: 22.32°S).

22.32°S). The Boa Vista station is closer to the region of the observed MSTIDs (selected area indicated by the square box in Figure 1) in the Northern Hemisphere than the Campo Grande station. This is because there is no digisonde instrument closer to the region at the southern region. Figures 7 and 8, from top-to-bottom, depict the temporal variation of the height of the *F* region at 6–9 MHz frequencies *(hF)* and corresponding Δh variation. The Δh is defined as the h deviation from the best fitted h at each frequency. According to *Lanchester et al*. [1993] and *Hocke and Schlegel* [1996], one can verify TID by exploring data from two frequencies and checking if they show downward phase motion.

In both Figures 7 and 8, it is possible to note the presence of AGW as shown by the downward propagation in the Δh (Δh is calculated using similar method for ΔTEC as represented by equation (1)) at both hemispheres (i.e., at Boa Vista and Campo Grande stations). The gravity wave activities show similar amplitudes and oscillations at both locations as illustrated by downward propagations. It is also important to note that the MSTIDs events activities in the Northern and Southern Hemispheres, which begin to appear around ~12.50 UT on all days, coincide with the appearance of the downward phase propagation of Δh shown by Figures 7 and 8 at Boa Vista and Campo Grande, respectively. These observations give consistent support on the possible association between AGWs and MSTIDs.

4.2. Daytime *F* Region Electric Field Mapping

The mechanism responsible for the daytime electrified MSTIDs could be similar to the generating mechanism during nighttime if the *E* region is not completely short circuited (i.e., if the *F* region controls). The conventional perception is that there is always short circuit effect in the *E* region during daytime which would not allow the mapping of polarization electric field to conjugate region. Nevertheless, this is not always the case as recently shown by *Abdu et al*. [2015].

Abdu et al. [2015] observed polarization electric field in the *F* region during the time interval of 13 to 21 LT and investigated the phenomenon by using the SUPIM model (Sheffield University Plasmasphere Ionosphere Model) simulation results to calculate the field line-integrated conductivity ratio. The polarization electric field is given by the following equation:

$$\vec{E}_y = -\Delta\vec{U}_z \times \vec{B}_o \left[\sum_F \Big/ \left(\sum_F + \sum_E \right) \right] \tag{3}$$

where E_y is the zonal polarization electric field, ΔU_z is the vertical perturbation wind, $\vec{B}_o$ is the magnetic field intensity, $\sum_F$ and $\sum_E$ are the field line-integrated Pedersen conductivities of *F* and *E* regions, respectively.

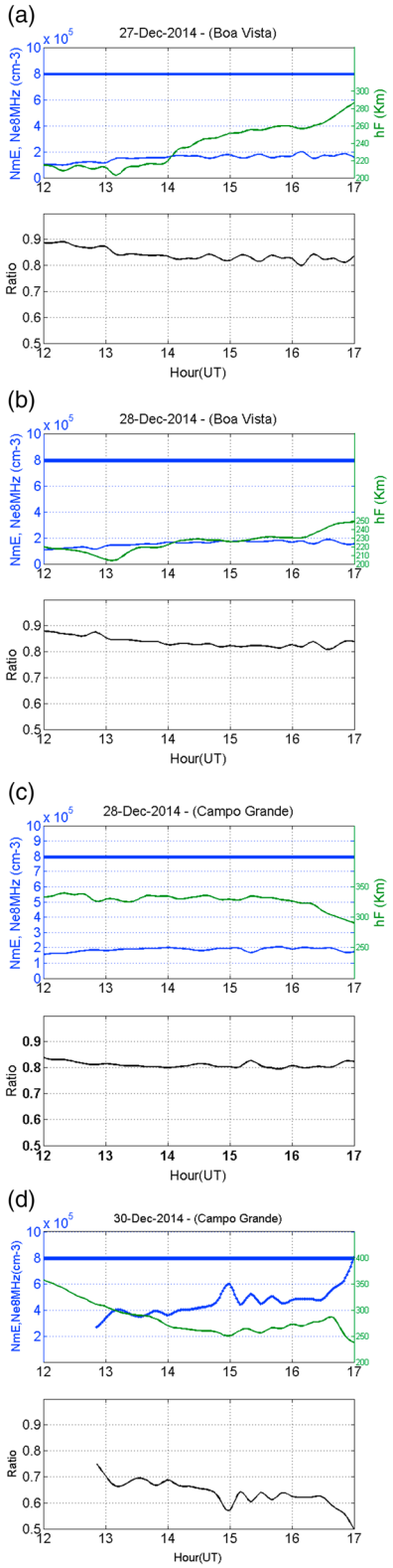

Figure 9. Electron density (thick blue) at the *F* region plasma frequency of 8 MHz (Ne8 MHz), the heights at 8 MHz plasma frequency (green curve), and the *E* layer peak density (NmE) (thin blue curve), as well as the ratio of Ne8MHz/(Ne8MHz + NmE) (black curve at the bottom plots for each day). (d) The same as Figure 6 but for day 30.

In their methodology they show that equation (4) can be used as a rough approximation of the local time (LT) variation of the integrated conductivity ratio,

$$\left[\frac{\sum_F}{(\sum_F+\sum_E)}\right] \approx \left[\frac{\mathrm{Ne8MHz}}{(\mathrm{Ne8MHz}+\mathrm{NmE})}\right] \quad (4)$$

where Ne8MHz is the electron density at the *F* region plasma frequency of 8 MHz and NmE is the *E* layer peak density. These parameters are obtained from digisonde.

Their results on both observation and simulation show that the zonal polarization electric field produced by the gravity wave wind perturbation in the *F* region is sustained when the conductivity ratio (in bracket on equation (3)) is around 0.8 (80%).

Based on the above methodology, we used the parameters Ne8MHz and NmE from the digisondes at magnetically conjugate sites of Boa Vista (2.62°N, 60.7°W, dip latitude: 4.74°N) and Campo Grande (20.55°S, 54.7°W, dip latitude: 12.38°S) to further investigate our results on daytime MSTIDs and electric field mapping to conjugate hemisphere (or electrified MSTIDs). The stations are shown in shaded red circle in Figure 1.

In Figure 9 the following parameters are plotted: Ne8MHz, the electron density at the *F* region plasma frequency of 8 MHz, the values of its heights (hF8MHz) and those of the *E* layer peak density (NmE) for days 27 and 28 December 2014 (the available days) over both Boa Vista and Campo Grande, as well as the rough approximation of the conductivity ratio, Ne8MHz/(Ne8MHz + NmE) (in the bottom plots for each day).

It is possible to observe from the bottom panels of Figures 9a–9c

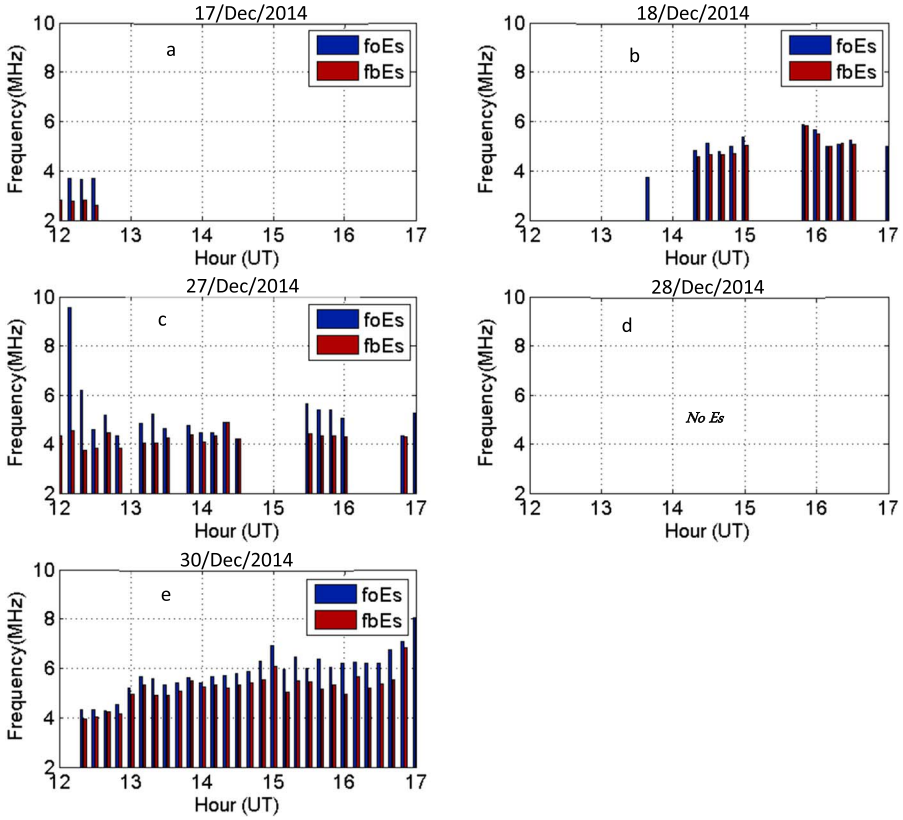

Figure 10. Histograms of f_oE_s (blue) and f_bE_s (red) from Campo Grande (54.7°W, 20.5°S) for days 17, 18, 27, 28, and 30 December 2014.

that the curve representing the rough approximation of the conductivity ratios are between 0.88 to 0.80, which means that approximately 80% zonal polarization electric field is produced by the gravity wave wind perturbation in the *F* region during the observed conjugate daytime electrified MSTID events. To support this hypothesis, we show at Figure 9d similar results of Figures 9a–9c but for day 30 December 2014, a day without electrified MSTIDs (which implies that there were no electric field mapping to the conjugate *F* region on this day). Figure 9d shows that the rough approximation for the conductivity ratio on this day dropped from less than 0.8 (around 12 UT) to 0.5 (around 17 UT). This daytime characteristic of conductivity ratio implies that, similar to nighttime polarization electric field mapping, the daytime gravity wave-induced electric field in the daytime *F* region could be responsible for the observed daytime electrified MSTIDs at conjugate region. In the paragraphs that follow, further investigation is carried out to drive home our arguments on the possible electric field *F* region conjugate mapping during daytime.

It is well known that the *E* layer of the ionosphere is sometimes attributed to the presence of enhanced ionized density known as the sporadic *E* (Es) [*Rishbeth and Garriott*, 1969]. This layer sometimes could also account for much higher density known as blanketing type sporadic *E* (Esb) which could sufficiently block the upper ionospheric *F* layer from radio wave propagation and causes the disappearance of the *F* trace in an ionogram [*Tsunoda*, 2008]. During this period of blanketing type Esb, the electric field in the *F* region is totally short circuited due to the very large conductivity in the geomagnetically connected *E* region, and as a consequence, the *F* conductivity at this period is expected to be very low (compared to the *E* region conductivity) such that electric field in the *F* region is minimum and mapping of electric field from one hemisphere to the other in the *F* region would be impossible. On this basis, in the following discussion, we investigate this above hypothesis as a possible evidence of the daytime electrified MSTIDs mechanism.

To prove the above hypothesis, we use the critical frequency of Es layer (f_oE_s) and the blanketing frequency of the Es layer (f_bE_s). The f_bE_s corresponds to the frequency from which the reflections from a higher layer than the Es layer begins to appear. This allows us to determine if there are strong or weak Es during the period of

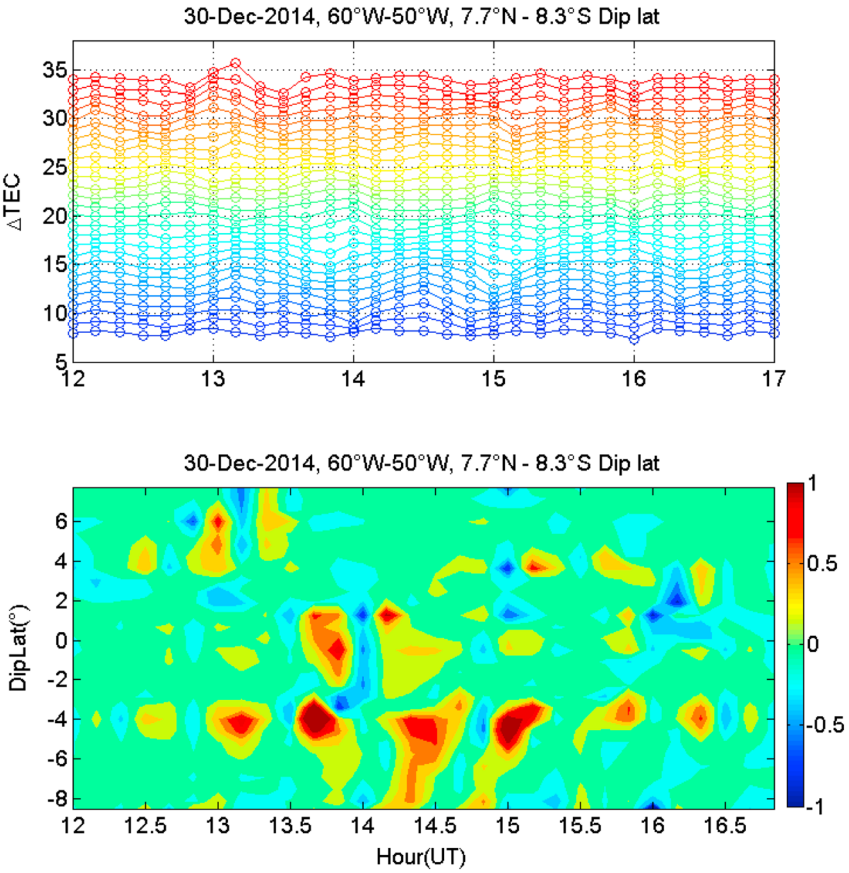

Figure 11. MSTIDs activity on 30 December 2014 showing no clear MSTIDs mapping.

the observed MSTIDs mappings (i.e., 12–17 UT). The results of f_oE_s and f_bE_s for 17, 18, 27, 28, and 30 December 2014, which correspond to days with electrified/mirrored MSTIDs at conjugate region (17, 18, 27, and 28) and the day without electrified/mirrored MSTIDs (30), are shown in Figure 10.

Figures 10a–10d show weak activities of Es during the period of the electrified MSTIDs on days 17, 18, 27, and 28, respectively. On the other hand, Figure 10e shows strong Es activity and no electrified/mirrored MSTIDs activity during this same day (30 December 2014), as show in Figure 11, providing clear evidence that the strong Es activity overwhelmed the *F* region conductivity and prevented the $\overrightarrow{E}_p$ generation/mapping at the *F* region during the period.

5. Conclusions

1. Using the network of GNSS receivers and digisonde instruments over the Brazilian sector, we investigate the spatial and time variability of daytime electrified MSTID and the mechanism involved in daytime electric field mapping to conjugate hemisphere.
2. Experimental daytime electrified MSTIDs at conjugate hemispheres are observed for the first time over the Brazilian sector.
3. MSTIDs generated in Southern Hemisphere or Northern Hemisphere mirrored in the conjugate hemisphere are caused by gravity wave-induced electric fields which map from one hemisphere and generate the mirrored MSTIDs in the conjugate region
4. We show that with the partial absence of *E* region short circuiting, mapping of polarization electric field from *E* region to *F* region is possible as well as electric field generation in the *F* region during daytime. This electric field mapping along the magnetic field lines would generate the MSTIDs at the conjugate region (which we referred to as electrified MSTIDs) as observed in our results.

5. The investigations in this study also show that *F* region magnetic field-aligned integrated conductivity should have more influence than *E* region conductivity during the mapping periods.

Acknowledgments
Jonah O.F. and E.R. de Paula would like to acknowledge the support from Conselho Nacional de Desenvolvimento Científico e Tecnológico (CNPq) under process 133429/2011-3 and 305684/2010-8 grants, respectively. E.A. Kherani is grateful to FAPESP under process 2011/21903-3. The authors also acknowledge Inez Batista for the Digisonde data.

References

Abdu, M. A. (2005), Equatorial ionosphere–thermosphere system: Electrodynamics and irregularities, *Adv. Space Res.*, *35*, 771–787.

Abdu, M. A., J. R. de Souza, E. A. Kherani, I. S. Batista, J. W. MacDougall, and J. H. A. Sobral (2015), Wave structure and polarization electric field development in the bottomside *F* layer leading to postsunset equatorial spread *F*, *J. Geophys. Res. Space Physics*, *120*, 6930–6940, doi:10.1002/2015JA021235.

Burnside, R. G., J. C. G. Walker, R. A. Behnke, and C. A. Gonzales (1983), Polarization electric fields in the nighttime *F* layer at Arecibo, *J. Geophys. Res.*, *88*(A8), 6259–6266, doi:10.1029/JA088iA08p06259.

Duly, T. M., J. D. Huba, and J. J. Makela (2014), Self-consistent generation of medium-scale traveling ionospheric disturbances (MSTIDs) within the SAMI3 numerical model, *J. Geophys. Res. Space Physics*, *119*, 6745–6757, doi:10.1002/2014JA020146.

Fritts, D. C., and M. J. Alexander (2003), Gravity wave dynamics and effects in the middle atmosphere, *Rev. Geophys.*, *41*(1), 1003, doi: 10.1029/2001RG000106.

Fukushima, D., K. Shiokawa, Y. Otsuka, and T. Ogawa (2012), Observations of equatorial nighttime medium-scale traveling ionospheric disturbances in 630-nm airglow images over 7 years, *J. Geophys. Res.*, *117*, A10324, doi:10.1029/2012JA017758.

Hocke, K., and K. A. Schlegel (1996), Review of atmospheric gravity waves and travelling ionospheric disturbances: 1982–1995, *Ann. Geophys.*, *14*, 917–940, doi:10.1007/s00585-996-0917-6.

Huba, J. D., D. P. Drob, T. W. Wu, and J. J. Makela (2015), Modeling the ionospheric impact of tsunami-driven gravity waves with SAMI3: Conjugate effects, *Geophys. Res. Lett.*, *42*, 5719–5726, doi:10.1002/2015GL064871.

Jonah, O. F., E. A. Kherani, and E. R. De Paula (2016), Observation of TEC perturbation associated with mediumscale traveling ionospheric disturbance and possible seeding mechanism of atmospheric gravity wave at a Brazilian sector, *J. Geophys. Res. Space Physics*, *121*, 2531–2546, doi:10.1002/2015JA022273.

Kotake, N., Y. Otsuka, T. Tsugawa, T. Ogawa, and A. Saito (2007), Statistical study of medium-scale traveling ionospheric disturbances observed with the GPS networks in Southern California, *Earth Planets Space, 59*, 95–102.

Kelley, M. C., and S. Fukao (1991), Turbulent upwelling of the mid-latitude ionosphere: 2. Theoretical framework, *J. Geophys. Res.*, *96*, 3747–3753.

Lanchester, B. S., T. Nygren, M. J. Jarvis, and R. Edwards (1993), Gravity wave parameters measured with EISCAT and Dynasonde, *Ann. Geophys.*, *11*, 925–936.

Martinis, C., J. Baumgardner, J. Wroten, and M. Mendillo (2010), Seasonal dependence of MSTIDs obtained from 630.0 nm airglow imaging at Arecibo, *Geophys. Res. Lett.*, *37*, L11103, doi:10.1029/2010GL043569.

Otsuka, Y., K. Shiokawa, T. Ogawa, and P. Wilkinson (2004), Geomagnetic conjugate observations of medium-scale traveling ionospheric disturbances at midlatitude using all-sky airglow imagers, *Geophys. Res. Lett.*, *31*, L15803, doi:10.1029/2004GL020262.

Rishbeth, H., and O. K. Garriott (1969), Some ionospheric phenomena, in *Introduction to Ionospheric Physics*, pp. 201–206, Academic Press, New York.

Tsunoda, R. T. (2008), On blanketing sporadic *E* and polarization effects near the equatorial electrojet, *J. Geophys. Res.*, *113*, A09304, doi:10.1029/2008JA013158.

Perkins, F. (1973), Spread *F* and ionospheric currents, *J. Geophys. Res.*, *78*, 218–226, doi:10.1029/JA078i001p00218.

Vadas, S. L. J., and A. Liu (2009), Generation of large-scale gravity waves and neutral winds in the thermosphere from the dissipation of convectively generated gravity waves, *J. Geophys. Res.*, *114*, A10310, doi:10.1029/2009JA014108.

Valladares, C. E., and R. Sheehan (2016), Observations of conjugate MSTIDs using networks of GPS receivers in the American sector, *Radio Sci.*, *51*, 1470–1488, doi:10.1002/2016RS005967.

Yigit, E., and A. S. Medvedev (2015), Internal wave coupling processes in Earth's atmosphere, *Adv. Space Res.*, *55*, 983–1003, doi:10.1016/j.asr.2014.11.020.